



HHS Public Access

Author manuscript

Neuroimage. Author manuscript; available in PMC 2018 December 01.

Published in final edited form as:

Neuroimage. 2017 December ; 163: 459–470. doi:10.1016/j.neuroimage.2017.09.004.

Mapping the complex topological organization of the human parietal face area

Ruey-Song Huang^{1,*}, Ching-fu Chen², and Martin I. Sereno^{3,4}

¹Institute for Neural Computation, University of California, San Diego, La Jolla, CA 92093, USA

²Department of Electrical and Computer Engineering, University of California, San Diego, La Jolla, CA 92093, USA

³Birkbeck/UCL Centre for NeuroImaging (BUCNI), London WC1E 7HX, UK

⁴Department of Psychology and Neuroimaging Center, San Diego State University, San Diego, CA 92182, USA

Abstract

The macaque monkey ventral intraparietal area (VIP) contains neurons with aligned visual-tactile receptive fields anchored to the face and upper body. Our previous fMRI studies using standard head coils found a human parietal face area (VIP+ complex; putative macaque VIP homologue) containing superimposed topological maps of the face and near-face visual space. Here, we construct high signal-to-noise surface coils and used phase-encoded air puffs and looming stimuli to map topological organization of the parietal face area at higher resolution. This area is consistently identified as a region extending between the superior postcentral sulcus and the upper bank of the anterior intraparietal sulcus (IPS), avoiding the fundus of IPS. Using smaller voxel sizes, our surface coils picked up strong fMRI signals in response to tactile and visual stimuli. By analyzing tactile and visual maps in our current and previous studies, we constructed a set of topological models illustrating commonalities and differences in map organization across subjects. The most consistent topological feature of the VIP+ complex is a central-anterior upper face (and upper visual field) representation adjoined by lower face (and lower visual field) representations ventrally (laterally) and/or dorsally (medially), potentially forming two subdivisions VIPv (ventral) and VIPd (dorsal). The lower visual field representations typically extend laterally into the anterior IPS to adjoin human area AIP, and medially to overlap with the parietal body areas at the superior parietal ridge. Significant individual variations are then illustrated to provide an accurate and comprehensive view of the topological organization of the parietal face area.

*Address correspondence to: Ruey-Song Huang, Institute for Neural Computation, University of California, San Diego, 9500 Gilman Dr. #0559, La Jolla, CA 92093-0559, Phone/fax: (858) 822-5977, rhuang@ucsd.edu.

Publisher's Disclaimer: This is a PDF file of an unedited manuscript that has been accepted for publication. As a service to our customers we are providing this early version of the manuscript. The manuscript will undergo copyediting, typesetting, and review of the resulting proof before it is published in its final citable form. Please note that during the production process errors may be discovered which could affect the content, and all legal disclaimers that apply to the journal pertain.

Keywords

near-face space; superior parietal cortex; multisensory maps; human VIP+ complex; topological models

Introduction

One of the primary functions of the posterior parietal cortex (PPC) is to integrate information across different sensory modalities. Single-unit recording studies have shown that neurons in the macaque ventral intraparietal area (VIP) respond to visual, tactile, auditory, and vestibular stimulation (Avillac et al., 2005, 2007; Bremmer et al., 2002; Chen et al., 2011; Colby et al., 1993; Duhamel et al., 1991, 1998; Schlack et al., 2005). In particular, area VIP contains neurons with aligned visual-tactile receptive fields (RFs) that are anchored to different regions on the face and upper body (Duhamel et al., 1991, Duhamel et al., 1998). However, detailed cortical maps of these bimodal RFs in macaques have been difficult to establish because of: (1) the location at the fundus of the intraparietal sulcus (IPS), (2) the small extent - about 5 mm in each dimension, and (3) unavoidable uncertainty in precisely locating depth electrode recording locations across long-lasting chronic awake-behaving recording experiments. Nevertheless, more recent studies in macaques have hinted that there might be multiple subdivisions of macaque VIP (Gattass et al., 2005; Guipponi et al., 2013; Lewis and Van Essen, 2000a, 2000b; Patel et al., 2010).

In humans, a region in the IPS was found to respond to visual, tactile, and auditory motion stimuli in functional magnetic resonance imaging (fMRI) experiments (Bremmer et al., 2001). We subsequently identified a multisensory parietal face area (a putative human homologue of macaque area VIP) in a similar though slightly more superior location, extending between the superior postcentral sulcus and the anterior IPS, by presenting wide-field videos and optic flow stimuli immediately in front of the subject's face and by delivering air puffs to randomized locations on the face in fMRI experiments (Huang and Sereno, 2007; Sereno and Huang, 2006). We then used phase-encoded paradigms (Engel, 2012; Sereno et al., 1995) to further define the rough retinotopic and somatotopic organization within that area. A direct overlay of visual and tactile maps on the same cortical surface revealed at least one aligned multisensory representation of the contralateral visual hemifield and contralateral hemiface in each hemisphere (e.g., the lower right visual field representation overlaps with the right chin, and so on upward in the visual field and on the face). Initial evidence suggested that this area might contain multiple aligned visual-tactile representations (e.g., see Subject 2 in Fig. 4 and Subject 6 in Fig. 6 in Sereno and Huang, 2006). However, the imaging resolution ($3.1 \times 3.1 \times 4$ mm voxels) in our previous studies was insufficient to discern the subdivisions in all of the subjects (see Supplementary material). While it is straightforward to acquire functional images at a higher spatial resolution (e.g., $2 \times 2 \times 2$ mm or smaller voxels), the signal-to-noise ratio (SNR) in periodic fMRI signals drops significantly with smaller voxels when using standard head coils in 3 Tesla MRI scanners (Hoffmann et al., 2009). In phase-encoded mapping experiments, successful reconstruction of detailed retinotopic or somatotopic maps depends on precise estimation of the phase angles of periodic signals with high SNR in individual voxels (Chen et al., 2017).

This makes mapping in small, higher-level cortical regions particularly challenging because the SNR there is generally lower than that in the early unisensory areas.

In this study, we developed surface coil arrays to refine the detailed topological organization within the human parietal face area with a spatial resolution and SNR higher than is typically achieved by using standard head coils in 3 Tesla scanners. The smaller-sized (resulting in higher SNR) surface coil arrays were placed directly over the superior parietal region (resulting in additional SNR increase from increased proximity to the cortex) to compensate for the loss of SNR due to much smaller voxel volume and then hand-tuned individually for each subject. In the first experiment, an MR-compatible tactile stimulation device (the 12-channel air-puff “Dodecapus” manifold in Huang and Sereno, 2007) was mounted above the surface coils to deliver phase-encoded tactile stimuli around the face. In the second experiment, phase-encoded looming visual stimuli were projected onto a wide-field direct-view screen while phase-encoded tactile stimuli were delivered to the face via a wearable mask containing built-in air tubes and nozzles (Chen et al., 2017; Huang et al., 2012). These experiments clearly revealed one and often two or more subdivisions within the parietal face area across hemispheres and subjects. Intersubject spherical morphing and surface-based complex-valued group-averaging techniques were used to summarize the location and extent of the parietal face area in relation to neighboring unisensory and multisensory areas in the superior parietal cortex. To demonstrate interhemispheric and intersubject variability in the topological organization of the parietal face area, we compare results from the current study with single-subject maps (most previously unpublished) from our previous studies acquired using standard head coils (Huang and Sereno, 2007, 2013; Huang et al., 2012; Sereno and Huang, 2006). Finally, we construct a set of topological models of the parietal face area to illustrate consistent and variable topological features observed within and across subjects.

Materials and Methods

Participants

Ten healthy adults (age 20-42, 5 female) with normal or corrected-to-normal vision participated in the new high-SNR surface-coil experiments. All subjects gave informed consent according to protocols approved by the Human Research Protections Program of the University of California, San Diego (UCSD). Five subjects (3 female) participated in Experiment 1, and the other five subjects (2 female) participated in Experiment 2. Data of two subjects in Experiment 2 were rejected due to severe motion artifacts or absence of significant activation in both hemispheres. For comparison with data acquired using standard 8-channel head coils, the Supplementary material includes published and unpublished single-subject maps from our previous studies (Huang and Sereno, 2007, 2013; Huang et al., 2012; Sereno and Huang, 2006). In total, visual and/or tactile maps of 26 distinct subjects are illustrated in this study.

Devices

We built MR-compatible devices to allow radio-frequency signal acquisition to be integrated with tactile and visual stimulation on and near the face (Fig. 1; for details of tactile

stimulation devices, see Huang and Sereno, 2007 and Huang et al., 2012). The signal acquisition system consisted of two 8-cm receive-only surface coils, a figure-8 passive detuning coil, and a bank of 8 preamplifiers (Fig. 1C; designed and fabricated by Larry May, development engineer at the UCSD Center for fMRI). The two-element surface coils were mounted symmetrically on the back of a baseball helmet (with its anterior part cut off) anchored to a supporting cradle. To reduce signal crosstalk between the two surface coils, the figure-8 coil was situated over them, partially overlapping both. The locations of active surface coils were determined empirically and iteratively in multiple pilot structural scans to ensure maximum image intensity in bilateral superior parietal cortex across subjects (Fig. 1D). Before each fMRI session, surface coils were individually fine-tuned while the subject was on a scanner bed pulled out of the MRI room. During the tuning of coil #1, radio-frequency reflection from coil #2 was attenuated by shorting it with a 50-ohm terminator. Variable capacitors on coil #1 were tuned using a spectrum analyzer (HP 8565A, Hewlett Packard) to achieve a maximum signal gain at the resonance frequency (peak at 127.72 MHz of our nominal 3-Tesla MRI scanners). The tuning procedure was then applied to coil #2 while coil #1 was being shorted. This back-and-forth procedure was repeated until maximum possible gain on both coils was achieved. Subject-specific hand-tuning of coils provides third, independent SNR advantage over standard head coils (beyond SNR increases due to a smaller coil size and closer placement to the cortex).

Experimental Design and Setup

Experiment 1—Somatotopic organization within the parietal face area was mapped using phase-encoded stimuli delivered by the Dodecapus tactile stimulation system (Huang and Sereno, 2007). The Dodecapus manifold was firmly mounted above the helmet on a base bolted down to the supporting cradle (Fig. 1A and C). The subject lay supine on the scanner bed with his/her head tilted forward (supported by foam padding underneath the head and neck) inside the helmet. Each “leg” (Loc-Line Modular Hose; Lockwood Products, Inc., OR) of the Dodecapus manifold was manually adjusted to aim its nozzle at one of twelve locations evenly distributed around the face, avoiding the eyes, nose, and mouth (locations #1 to #12 in Fig. 1B). In each of two repeated 512-s scans, a sequence of air puffs (with gaps between successive puffs) was delivered to location #1 at the left forehead for 5.33 s, and then to each of the subsequent locations (locations #2 to #12) within a 64-s cycle (8 cycles total). Within each 5.33-s period at each location, each 100-ms air puff was followed by a gap of 100 ms (80% probability) or 200 ms (20% probability). At the end of each 5.33-s period, an incomplete air puff or gap was terminated at the current location, and a full 100-ms air puff was delivered to the next location. Before the subject was moved into the scanner bore, tactile stimuli were tested for at least a full cycle to ensure that they could be clearly felt at each location on the face. The air puffs were described by subjects as easily detectable but pleasant. During functional scans, all subjects were instructed to close their eyes in complete darkness and covertly attend to the pulsation pattern and the locations of air puffs on their face.

Experiment 2—In the second experiment, retinotopic and somatotopic organization within the parietal face area was mapped in four 512-s scans (two visual followed by two tactile scans) within the same fMRI session. To prevent occlusion and clear near-face space for a

close-up screen, phase-encoded tactile stimuli (air puffs) were delivered to 12 locations around the face via plastic tubes embedded on a wearable mask custom molded for each subject (Fig. 1B and C; Chen et al., 2017; Huang et al., 2012). Each mask was made of X-Lite thermoplastic sheets with a grid of -0.5×0.5 cm. Flexible air tubes were attached to the outside of the mask and were each terminated with an elbow fitting (Part No. FTTP-L210NP; Omega Engineering, Inc., OR) to redirect airflow perpendicularly to the face through a mesh opening. The open end of the elbow was approximately 5 mm above each stimulation site on the skin of the face. The other end of each tube was connected via quick connectors (Part No. SMM01, SMF01; Colder Products Company, MN) to a bundle of 25-ft tubes, which extended through a wave guide and then connected to the stimulus control system located in the MRI console room (see Fig. S1 in Huang et al., 2012). Fiducial points marked on the mask during face molding were used to precisely align them with the corresponding points on the face (e.g., eyebrows) during experimental setup. After testing tactile stimuli on the face for at least a full cycle, the subject was moved to the isocenter within the scanner bore and a direct-view screen was then installed about 15 cm directly in front of the subject's eyes. Visual stimuli were back-projected by an LCD projector (Dell 3300MP; 1024×768 pixels) onto a 35×26 cm screen region, yielding a field of view of $\sim 100 \times 80^\circ$. In each of two repeated visual scans, phase-encoded looming balls appeared at a polar angle that advanced in a counterclockwise direction periodically (Supplementary Figure S1; also see details in Methods – Visual Mapping Paradigm and Fig. S6 in Huang et al., 2012). Subjects were instructed to fixate a central cross while attending to each looming ball apparently passing by their faces. Subjects were also required to press a key on a fiber-optic response pad (Current Designs, Inc.) when a white ball randomly turned red in 20% of all trials. All apparatus and setup remained unchanged following two visual scans, except that the projector was turned off. In each of two repeated tactile scans, tactile stimuli with the same design and parameters as in Experiment 1 were then delivered to the face via the mask while the subject closed his/her eyes in complete darkness.

In both experiments, compressible foam padding was firmly inserted into the gap between the head and the helmet to restrict head movements. All subjects had previously participated in multiple sessions of fMRI experiments and were experienced in remaining motionless without using a bite-bar. Subjects were instructed to attempt to remain motionless in the helmet during the entire scanning session.

Data acquisition

Subjects were scanned in a General Electric 3-T scanner at the UCSD Center for Functional MRI. Each subject participated in an fMRI session consisting of 2-4 functional scans and one anatomical alignment scan, which were all acquired using the custom-built surface coils (Fig. 1C). Functional images were acquired with a single-shot echo-planar imaging (EPI in Fig. 1D; bandwidth = 62.5 kHz) pulse sequence with the following parameters: (1) Experiment 1: TR = 2 s, TE = 35.4 ms, flip angle = 90° , FOV = 200×200 mm, 16 axial slices, thickness = 2.6 mm, gap = 0 mm, in-plane voxel size = 1.56×1.56 mm, matrix = 128×128 , 256 images per slice (512 s per scan); (2) Experiment 2: TR = 2 s, TE = 35.9 ms, flip angle = 90° , FOV = 192×192 mm, 15 axial slices, thickness = 2.4 mm, gap = 0 mm, in-plane voxel size = 1.5×1.5 mm, matrix = 128×128 , 256 images per slice (512 s per scan). In

both experiments, alignment images were acquired at the same orientation as functional images by a fast spoiled gradient echo (FSPGR) pulse sequence: FOV = 256×256 mm, 106 axial slices, thickness = 1.3 mm, in-plane voxel size = 1×1 mm, and matrix = 256×256 (T1W_a in Fig. 1D). In a different session, each subject was scanned using a standard 8-channel head coil, and two sets of high-resolution structural images were acquired by an FSPGR pulse sequence with parameters: FOV = 256×256 mm, 160 axial slices, voxel size = 1×1×1 mm, and matrix = 256×256 (T1W in Fig. 1D). For each subject, cortical surfaces were reconstructed from the registered average of these two image sets using the FreeSurfer package (Dale et al., 1999; Fischl et al., 1999a).

Data analysis

Functional images were motion-corrected and then registered to the last functional scan immediately before the alignment scan using the 3dvolreg tool of the Analysis of Functional Neuroimages (AFNI) package (Cox, 1996). For each voxel, a time-point-wise average was applied to the time series (256 sample points) of two repeated functional scans of the same stimulation modality. For each voxel, linear trends were removed from the averaged time series (256 sample points), and a power spectrum (128 bins between 0-127 cycles/scan) was obtained by discrete Fourier transform:

$$X_m(\omega) = \sum_{t=1}^{256} x_m(t)e^{-j\omega t} = |X_m(\omega)| e^{j\theta_m(\omega)}, \quad (1)$$

in which $x_m(t)$ is the time series in voxel m , and $X_m(\omega)$, $|X_m(\omega)|$, and $\theta_m(\omega)$ are the complex component, amplitude, and phase angle at frequency ω . The “signal” in the power spectrum is defined as the complex component at the stimulus frequency ($\omega_s = 8$ cycles/scan) while the “noise” is defined as the complex components at the remaining frequencies ($\omega_n = 0-127$ cycles/scan; excluding 0-2, 7-9, 15-17, 23-25, and 32 cycles/scan). For a voxel m , an F -statistic (F_m) was estimated from the ratio between the signal energy $|X_m(\omega_s)|^2$ and the average of noise energy $|X_m(\omega_n)|^2$:

$$F_m = \frac{|X_m(\omega_s)|^2 / df_s}{\left(\sum_{\omega_n} |X_m(\omega_n)|^2\right) / df_n}. \quad (2)$$

A p -value was then estimated by considering the degrees of freedom (df) of signal ($df_s = 2$ for real and imaginary parts at the stimulus frequency) and noise ($df_n = 230$ for the remaining frequencies) in F_m . For a voxel m , a complex number ($F_{m,r}$, $F_{m,i}$) incorporating both F -statistic and phase angle, $\theta_m(\omega)$, was computed by $F_{m,r} = f_m \cos(\theta_m(\omega))$ and $F_{m,i} = f_m \sin(\theta_m(\omega))$, where f_m is the square root of F_m . Voxels with an F -statistic higher than a single threshold were selected and projected onto corresponding vertices on the cortical surfaces using FreeSurfer. The phase angle, $\theta_m(\omega)$, and f_m of each vertex were indicated by

color hue and saturation, according to a color wheel representing the contralateral hemiface (or visual hemifield) (Figs. 2 and 3).

The distribution of signal phase angles within each sROI is characterized using circular statistics (Chen et al., 2017). For a vertex v in an sROI r with V vertices corresponding to stimulus modality s , the phase angle, $\theta_{v,s}$, was first converted to the corresponding complex number, $z_{v,s} = \exp(j\theta_{v,s})$. The mean phase angle in this sROI, $\bar{\theta}_s^{(r)}$, was then obtained by (Fisher, 1993):

$$\bar{z}_s^{(r)} = \frac{1}{V} \sum_{v=1}^V z_{v,s} = \frac{1}{V} \sum_{v=1}^V \exp(j\theta_{v,s}) = \exp(j\bar{\theta}_s^{(r)}). \quad (3)$$

For vertices activated by both visual and tactile stimuli within an sROI, r , the association between the phase angles of two modalities, s_1 and s_2 , was described by a bimodal circular correlation coefficient, $\rho_{12}^{(r)}$, defined as (Jammalamadaka and SenGupta, 2001):

$$\rho_{12}^{(r)} = \frac{\sum_{v=1}^V \left[\sin(\theta_{v,s_1} - \bar{\theta}_{s_1}^{(r)}) \sin(\theta_{v,s_2} - \bar{\theta}_{s_2}^{(r)}) \right]}{\sqrt{\left[\sum_{v=1}^V \sin^2(\theta_{v,s_1} - \bar{\theta}_{s_1}^{(r)}) \right] \left[\sum_{v=1}^V \sin^2(\theta_{v,s_2} - \bar{\theta}_{s_2}^{(r)}) \right]}}. \quad (4)$$

A p -value of $\rho_{12}^{(r)}$ was then estimated from the distribution of $\sqrt{V} \frac{\sqrt{\hat{\lambda}_{20} \hat{\lambda}_{02}}}{\sqrt{\hat{\lambda}_{22}}}$ (Jammalamadaka and SenGupta, 2001), where

$$\hat{\lambda}_{ij} = \frac{1}{V} \sum_{v=1}^V \left[\sin^i(\theta_{v,s_1} - \bar{\theta}_{s_1}^{(r)}) \sin^j(\theta_{v,s_2} - \bar{\theta}_{s_2}^{(r)}) \right]. \quad (5)$$

When V is large, $\sqrt{V} \frac{\sqrt{\hat{\lambda}_{20} \hat{\lambda}_{02}}}{\sqrt{\hat{\lambda}_{22}}} \rho_{12}^{(r)}$ forms a standard normal distribution; thus, the significance of $\rho_{12}^{(r)}$ can be verified under the null hypothesis $\rho_{12}^{(r)} = 0$. If the phase angles of vertices in the overlapping region of an sROI r in response to two different stimulus modalities s_1 and s_2 are independent, $\rho_{12}^{(r)} = 0$; but the reverse may not be true.

Results

Surface coil performance and sROI measurement

The signal gain of each surface coil was individually tuned prior to each fMRI session, but the resulting functional images did not always exhibit exactly symmetric distribution of SNR in both hemispheres (Fig. 1D; also see surface-based SNR maps in Supplementary Figure

S2). In sessions where a comparable SNR was measured bilaterally, some subjects only show significant periodic activation ($p < 0.05$, uncorrected) at the superior parietal cortex in one hemisphere. While technical limits of coil tuning (e.g., intrinsic gain of electronic components) could partially account for the interhemispheric imbalance, it is common to observe that a higher-level topological area may be missing a partial to complete hemifield representation unilaterally in phase-encoded mapping experiments due to temporally uneven distribution of attention throughout the scan (e.g., see Hagler et al., 2007; Huang et al., 2012). Here, we only show positive results with somatotopic maps rendered on eight hemispheres of five subjects in Experiment 1 (Fig. 2), and aligned retinotopic and somatotopic maps rendered on three right hemispheres of three subjects in Experiment 2 (Fig. 3). Tables 1 and 2 summarize the peak activation location (Talairach coordinates), surface area, volume (voxels), and statistics for each sROI outlined in Figs. 2 and 3. Across subjects in both experiments, the parietal face area was identified as a contiguous region located at the superior postcentral sulcus, slightly extending onto the postcentral gyrus in some subjects. Across subjects, the surface area of each sROI ranges from 114 to 496 mm² (equivalent to a square area of about 10.7×10.7 to 22.3×22.3 mm), and the total volume of all voxels enclosed in each sROI ranges from 394 to 1276 mm³.

BOLD signal changes

Supplementary Figures S3 and S4 show time courses of blood-oxygen-level dependent (BOLD) signals averaged across voxels enclosed in each peak activation region (outlined in a thin yellow contour) within each sROI (outlined in a dashed black contour) in Figs. 2 and 3; also see measurements and statistics of sROIs in Tables 1 and 2. To better characterize the BOLD signal change in response to periodic stimulation, a waveform was reconstructed by inverse Fourier transforming the periodic components (harmonics: 8, 16, and 24 cycles per scan) on the power spectrum of the average BOLD signal in each peak activation region. Across subjects and stimulus modalities, the peak-to-peak signal change of the reconstructed periodic waveform (thick gray curves in Figs. S3 and S4) ranges from 0.74 to 2.59%. To demonstrate the maximum temporal SNR that surface coils can achieve, Supplementary Figures S5 and S6 show the original time course and a waveform reconstructed from the periodic components in a single voxel identified with the highest peak-to-peak signal change (ranging from 1.8 to 14.8%) within each peak activation region in Figs. 2 and 3.

Average location and extent

To illustrate intersubject variability in location and extent of the parietal face area in Figs. 2 and 3, activation maps of each subject were spherically morphed to the *fsaverage* sphere in FreeSurfer package using a sulcus-based criterion and then back-sampled to the cortical surfaces of a representative subject (Fig. 4A; see methods in Fischl et al., 1999b; Hagler et al., 2007). The contour of each sROI was outlined from each morphed map and then superimposed on the same cortical surface. Surface-based group-average maps of lip, face, finger, shoulder, and leg representations as well as maps of video-driven visual cortex from our other studies (Huang and Sereno, 2007, 2013, 2018; Huang et al., 2012) were back-sampled onto the same cortical surfaces in Fig. 4A. Across subjects, the parietal face area is consistently found at the superior part of the postcentral sulcus, where it extends anteriorly to border the finger (hand) representations in the primary somatosensory cortex (S-I) at the

superior postcentral gyrus; inferiorly and laterally to adjoin the parietal hand/finger area (human homologue of macaque anterior intraparietal area [AIP]; Borra et al., 2008; Culham et al., 2003; Guipponi et al., 2013; Jastorff et al., 2010); and medially/superiorly to overlap with the parietal body areas (PBA, including shoulder and leg representations; Huang et al., 2012). In the group-average visual maps (Fig. 4A), the parietal face area is located at the anteriormost end of the superior-parietal stream (one of the dorsal visual streams) activated by wide-field videos or simulated egomotion (Huang and Sereno, 2013, 2018; Huang et al., 2015; Sereno and Huang, 2014).

Topological organization

Results of topological mapping are illustrated in detail for one representative subject in each experiment (Figs. 2 and 3), and then compared within and across subjects in the following sections. In Experiment 1, the parietal face area in each hemisphere of Subject 1 is identified as a contiguous sROI showing significant periodic activation (thresholded at $F_{2,230} = 3.035$, $p = 0.05$, uncorrected) at the superior part of the postcentral sulcus (PoCS), as indicated by a red ellipse over the inflated cortical surface in lateral and dorsal-lateral views (Fig. 2). Its location among neighboring sulci is consistent across the left and right hemispheres. Detailed somatotopic organization in each sROI is shown in a close-up view of the superior parietal lobule (as indicated by a black square over the dorsal-lateral surface). Here, we consider each sROI a compound map (cluster) without delineating borders that separate its potential subdivisions. An arrow is used to illustrate a continuous polar-angle progression from the lower face (colored in green) to upper face (colored in red) representations on the cortical surface. The sROI in Subject 1's left hemisphere (LH) contains two clear contralateral hemiface subdivisions, with their upper face representations adjoining each other centrally and two separate lower face representations extending ventrally (laterally) and dorsally (medially), which are tentatively labeled VIPv (ventral) and VIPd (dorsal) (see Discussion). The sROI in Subject 1's right hemisphere (RH) contains two small hemiface subdivisions, with their upper face representations adjoining each other centrally and lower face representations extending ventrally (laterally) and dorsal-anteriorly. The ventral subdivision is consistent with subdivision VIPv in the left hemisphere, while the dorsal-anterior subdivision is less commonly observed across subjects (see topological types in Intersubject consistency and variability below).

In Experiment 2, the parietal face area in the right hemisphere of Subject 6 is identified as an sROI containing aligned retinotopic and somatotopic maps of contralateral visual-tactile space at the superior postcentral sulcus (as indicated by a red ellipse in Fig. 3). The topological organization within this sROI shows two separated upper visual field (upper face) representations and two separated lower visual field (lower face) representations, which form a total of four aligned visual-tactile subdivisions, including VIPd and VIPv (indicated by white arrows) and two additional subdivisions posterior to both (indicated by black arrows; see Discussion). The overall overlap between retinotopic and somatotopic maps within this sROI is 82.2%, as estimated by the percentage of surface vertices showing significant activation ($F_{2,230} > 3.035$, $p < 0.05$, uncorrected) in response to both visual and tactile stimuli (Table 2). The degree of polar-angle alignment between retinotopic and somatotopic maps within this sROI is 0.38 ($p < 4.03 \times 10^{-11}$, Bonferroni-corrected; Table 2),

which is a bimodal circular correlation coefficient estimated from the overlapping vertices (see Data analysis).

Intersubject consistency and variability

The topological organization of the parietal face area exhibited high interhemispheric and intersubject variability in a moderate-sized group of subjects scanned with a high SNR method. Subjects (hemispheres) showing consistent topological features are summarized in groups. First, Subjects 2 (RH), 3 (LH), and 5 (RH) show a major hemiface representation with the upper face located anterior to the lower face representation. Second, Subjects 1 (LH), 2 (LH), 4 (LH), 6 (RH), and 7 (RH) show at least two hemiface (or visual hemifield) representations, namely VIPv and VIPd, where their upper face representations adjoin each other centrally and two separate lower face representations extend ventrally (laterally) and dorsally (medially). Third, Subjects 1 (RH), 3 (RH), and 8 (RH) show complex organization inconsistent with either of the above two groups. These results confirm that the parietal face area contains one or more subdivisions, as suggested in our previous studies (Serenio and Huang, 2006, 2014).

To better model the complex topological organization of the parietal face area across subjects, we reanalyzed visual and/or tactile maps in 23 subjects from our previous studies (Huang and Sereno, 2007, 2013; Huang et al., 2012; Sereno and Huang, 2006). Five subjects overlapped with the current study, which allowed us to measure within-subject and between-coil-type variability (see Within-subject reproducibility). Maps of 26 distinct subjects from the current and previous studies are sorted by their topological features in each hemisphere, as shown in Supplementary Figures S7-S10 and summarized in Table 3. Within and across subjects, topological maps of the parietal face area (VIP+ complex) situated between the postcentral sulcus (PoCS) and intraparietal sulcus (IPS) are classified into two base types (Types 1.0 and 2.0), each with three subtypes (Fig. 4B). Without creating more types, we use “v” to indicate slight variations (adding or missing partial representations) on an existing base type or subtype; and use “none” to indicate unclassifiable maps (Figs. S7-S10 and Table 3). One of the commonly observed variations is a small lower face (or visual field) representation situated anterior to the upper face (or visual field) representation at the superior PoCS, as indicated by a dark-green crescent in Fig. 4B. For each base type and its subtypes, detailed topological features are illustrated as follows.

Type 1.0 exhibits a single hemiface (or visual hemifield) map with the upper face (or visual field) representation situated anterior to the lower face (or visual field) representation (e.g., Subject 9 in Figs. S7 and S8). The posterior lower face (or visual field) representation may extend dorsally (medially) to form Type 1.1 (e.g., Subject 5 in Fig. S8), or extend both dorsally (medially) and ventrally (laterally) to form Type 1.2 (e.g., Subject 11 in Fig. S9). Type 1.3 exhibits a second upper face (or visual field) representation situated posterior to a continuous strip of lower face (or visual field) representation, forming four lower-to-upper progressions (e.g., Subject 20 in Fig. S9). The anterior subdivisions of VIP+ complex are indicated by white arrows, while the posterior subdivisions are indicated by black arrows (Figs. 4B, S7-S10; see Discussion).

Type 2.0 exhibits a central upper face (or visual field) representation adjoined by two separate lower face (or visual field) representations ventrally (laterally) and dorsally (medially), e.g., Subject 1 in Fig. S7. Missing either one of the lower face (visual field) representations in Type 2.0 forms Type 2.1 (e.g., Subject 1 in Fig. S8) or Type 2.2 (e.g., Subject 22 in Fig. S9). Type 2.3 exhibits a second upper face (or visual field) representation situated posterior to the VIPd/VIPv complex in Type 2.0, forming four lower-to-upper progressions (e.g., Subject 18 in Fig. S9). Notably, Type 2.3 differs from Type 1.3 only in that its dorsal and ventral lower face (or visual field) representations are separated from each other (Fig. 4B; see Discussion).

Within-subject reproducibility

To demonstrate within-subject reproducibility of topological organization across sessions, we compare maps of the parietal face area acquired by surface coils (current study; in red boxes) and 8-channel head coils (previous studies; in blue boxes) within each of five subjects (Figs. S7-S10). In Subject 1, the sROI in either hemisphere shows roughly the same activation location and extent (dashed black contours) as well as consistent topological organization in somatotopic maps that were acquired using different kinds of coils in different sessions (paired LH maps in Fig. S7: Type 2.0; paired RH maps in Fig. S8: Type 2.1v). In Subject 2, the sROI in either hemisphere shows consistent activation location and extent across sessions (paired LH maps in Fig. S7; paired RH maps in Fig. S8). However, the ventral lower face representation is missing from the LH head-coil map (Type 2.2v; Fig. S7), which is present in the LH surface-coil map (Type 2.0v). In Subject 2's right hemisphere, the anterior portion the sROI (dashed black contours) shows a single subdivision that is consistent across sessions (both Type 1.0v in paired RH maps). In Subject 3, the left sROI shows consistent activation location across sessions (paired LH maps in Fig. S7). However, the surface-coil map subtends only the ventral (lateral) portion of the head-coil map (as indicated by dashed black contours), and shows two consistent lower-to-upper face progressions (an incomplete Type 2.3v map). The right sROI of Subject 3 subtends an elongated region across the superior PoCS, with a slight offset across sessions (paired RH maps in Fig. S8). However, neither map shows clear topological organization (Type: none). In Subject 5, the right sROI shows aligned activation location and extent as well as consistent topological organization across sessions (both Type 1.1; paired RH maps in Fig. S8). Additionally, the left sROI of Subject 4 shows a consistent activation location and extent (with a slight offset) as well as consistent topological organization (Type 2.0) across sessions and modalities (see surface-coil tactile map in Fig. S7 and head-coil visual map in Fig. S9; head-coil tactile map unavailable).

Discussion

Macaque area VIP

Topological mapping of higher level areas in the posterior parietal cortex of nonhuman primates is challenging for single-unit recording studies, especially in awake behaving animal experiments. In particular, macaque area VIP is a small region located at the fundus of the IPS, making it difficult to reconstruct a VIP map from numerous recording sites distributed across slices and recording sessions spread over months or years. Recent monkey

neuroimaging studies have begun to map detailed organization of the IPS at higher resolutions (~1.5 to 2 mm) and to display the results on inflated or flattened cortical surfaces (Guipponi et al., 2013; Patel et al., 2010).

High-resolution mapping with surface coils

In humans, the parietal face area occupies a cortical patch (sROI) of about 10×10 to 20×20 mm in the superior postcentral sulcus, and the total volume of voxels enclosed in each sROI is about 1000 mm³ or less, as suggested by data in the current study (Tables 1 and 2). The imaging resolution (e.g., 3.1×3.1×4 mm) used in our previous studies was insufficient to clearly resolve some of the subdivisions in the parietal face area (Figs. S7-S10; Huang and Sereno, 2007; Huang et al., 2012; Sereno and Huang, 2006). It is straightforward to increase the imaging resolution by reducing the in-plane voxel size and slice thickness. However, SNR in the fMRI time course is also reduced roughly proportional to voxel volume, everything else held constant (Buxton, 2009; Hoffmann et al., 2009). The voxel volumes in the current study are less than 1/6 of those in our previous studies. Small, closely-placed, and hand-tuned surface coils have three potential SNR advantages: (1) smaller-sized coils receive less noise from other parts of the brain; (2) coil placement closer to the brain increases signals; and (3) subject-specific coil tuning further boosts signal gain. These three factors help compensate for the loss of SNR at smaller voxel volumes. However, there are several potential factors (e.g., imbalanced signal gains, crosstalk between coils) that can reduce the SNR of coil arrays, which may account for the weak or absent activation unilaterally in some of the subjects (negative results not shown).

In subjects showing high SNR in the superior parietal cortex (Fig. S2), the peak activation region within each sROI shows a peak-to-peak signal change comparable to or higher than the 1-2% signal change commonly observed in fMRI experiments using standard voxel sizes (3-5 mm in each dimension). In this context, it is important to note that that all phase-encoded signals are essentially ‘subtractions’ – for a periodic signal to appear at all, one map position (polar angle) has to beat all other map positions. In each subject in Experiment 2, the peak activation regions in visual and tactile scans closely overlapped with each other and they both exhibited a large (differential) signal change with high statistical significance (Figs. 3, S4, S6; Table 2). This provides direct evidence for aligned visual-tactile representations in the parietal face area at a high spatial resolution (5.4 mm³ vs. standard 27-36 mm³ per voxel). This is, however, still too coarse a resolution to determine whether multisensory signals come from the same columns or neurons, as has nevertheless been found to be the case in single-unit studies.

Locating human area VIP

In recent human fMRI studies, a number of confusingly differently located and differently named locations in between the postcentral sulcus and the anterior IPS have been proposed as the site of a putative human homologue (pVIP) of macaque area VIP. We discuss these in two groups, posterior and anterior.

Several studies have used optic flow stimuli (i.e., visual-only stimuli) to activate multiple areas in or near the anterior IPS (IPS5 in Konen and Kastner, 2008; VIP in Wall and Smith,

2008; pVIP in Cardin and Smith, 2010; IPSmot in Pitzalis et al., 2013). Another study showed that an area located at the confluence of the anterior IPS and PoCS was activated by vibrotactile stimulation of the posterior neck muscles (VIP in Fasold et al., 2008; their left VIP appears more posterior than their right VIP). The locations of these five areas (four defined by visual stimuli only and one by vibrotactile stimuli only) overlap the posterior-lateral edge of the multisensory parietal face area identified in our previous and current studies (Sereno and Huang, 2006; Huang et al., 2012). However, none of these areas were shown to have aligned multisensory (visual and tactile) responses to stimuli near or on the face, which is critical to the functional definition of area VIP, as established by previous invasive studies in macaque monkeys (Avillac et al., 2005, 2007; Duhamel et al., 1998). In addition, the visual stimuli used in the human fMRI studies typically extended to only 10 degrees (or less) of eccentricity. Based on previous invasive studies in macaque monkeys, the use of these limited visual stimuli may have substantially underestimated the full extent of pVIP in humans.

Other studies have used either vibrotactile only or visual stimuli only (motion or videos) to activate a more anterior set of areas situated between the superior postcentral sulcus and the upper bank of the anterior IPS (e.g., antIPS in Sunaert et al., 1999; DIPSA in Orban et al., 2006 and Ferri et al., 2015; 2v in Fasold et al., 2008; p2v in Cardin and Smith, 2010; VIP in Smith et al., 2012; pVIP in Furlan et al., 2014; DIPS in Holt et al., 2014), which overlap the anterior-superior portion of the parietal face area as defined in our previous and current studies.

In sum, because multiple areas in the human IPS and PoCS have been found to respond to visual motion, including optic flow stimuli (e.g., Helfrich et al., 2013; Huang et al., 2015; Konen and Kastner, 2008; Orban et al., 2006; Pitzalis et al., 2013; Sunaert et al., 1999; and others), the location of the human parietal face area (or pVIP) can only be definitely confirmed if a visual-motion-responsive area also responds to tactile, auditory, and/or vestibular stimuli (e.g., Bremmer et al., 2001; Eger et al., 2015; Huang et al., 2012; Sereno and Huang, 2006).

Another confusing issue is the name VIP itself, the ventral intraparietal area. The name originally signified its location in the depths of the macaque monkey IPS. In humans, however, the relatively enlarged inferior parietal lobule (most notably the angular gyrus) results in a medial and posterior displacement of the posterior IPS areas (Sereno and Huang, 2014). Consequently, the probable human homologue of macaque lateral intraparietal area (LIP) is actually located on the “medial” bank of the IPS (Konen and Kastner, 2008; Sereno et al., 2001). Because the human parietal face area (pVIP) is situated somewhat anterior to the expanded angular gyrus, it has been displaced somewhat anteriorly but less further medially compared with the LIP+ (IPS-x; putative human homologues of macaque area LIP), so that it ends up being slightly lateral to LIP+ (Fig. 4A). However, despite these plastic deformations, the general neighbor relations between somatosensory cortex, multisensory cortex, and predominantly visual cortex are preserved.

In the current study, we used spherical morphing and complex-valued surface-based group map averaging techniques to summarize the location and extent of the topologically

organized parietal face area across subjects with respect to neighboring unisensory and multisensory areas on the same cortical surfaces (Fig. 4A). In the group-average visual maps, one of the dorsal visual retinotopic streams emanating from occipital cortex stretches along the IPS and ends at the parietal face area, which extends between the superior postcentral sulcus and the upper bank of anterior IPS (Huang and Sereno, 2013, Huang and Sereno, 2018). Sereno and Huang, 2014). Thus, from a retinotopic point of view, pVIP is the anterior-most set of a large number of retinotopic areas that extend all the way back to V1.

The anterior border of the human VIP+ complex as defined here essentially reaches the finger (hand) representations in S-I (areas 3a, 3b, 1, and 2). Though we could not completely rule out the possible presence of a thin area in between without additional, high resolution somatosensory mapping, its theoretical extent would have to be quite narrow. Moving laterally along the postcentral sulcus in the group-average tactile maps, the parietal face area is adjoined by a parietal finger/hand area important for grasping, the human homologue of macaque area AIP (Fig. 4A; Borra et al., 2008; Culham et al., 2003; Filimon et al., 2007, 2009; Guipponi et al., 2013; Jastorff et al., 2010). Finally, moving medially, the human VIP+ complex directly adjoins (in fact, slightly overlaps) the parietal body areas (including shoulder and leg representations; Huang et al., 2012), which extend up to the midline (Fig. 4A). The parietal finger/hand area is not typically activated by wide-field visual stimuli presented in eye-centered coordinates with the hands at rest alongside the body. The parietal body areas partially overlap the parietal face area and lower-field-driven multisensory cortex at the superiormost ridge of the superior parietal lobule. Taken together, the neighboring unisensory and multisensory areas (LIP+, AIP, S-I [fingers/hand], and parietal body areas in Fig. 4A) can be used to precisely define the location of the parietal face area, with its center located superior-medial to the anterior IPS and within the superior postcentral sulcus. Finally, the center of human parietal face area is more heavily myelinated than surrounding areas (Sereno et al., 2012) as originally recognized by Flechsig (1920).

Post-mortem studies have defined another set of differently named cortical areas that partly overlap the parietal face area as defined here. These include areas 7PC and 5L as defined by cytoarchitectonic mapping in humans (Scheperjans et al., 2008a, 2008b). Though these names are different, it is important to point out that no existing literature provides solid evidence for a second area in the human IPS with the necessary multisensory characteristics that define area VIP. Finally, recent dense microelectrode mapping experiments in S-I (3a, 3b, 1, 2) and area 5 summarized several competing parcellations of the IPS in macaque monkeys (Seelke et al., 2012). One way to avoid adding to the ever growing pile of names might be to define the human parietal face and body areas as homologous to macaque areas VIP and 5/PE combined (see Figure 1 in Seelke et al., 2012), which would fit in with them extending anteriorly to directly adjoin area 2 (in S-I) at the postcentral gyrus.

Models of topological organization

Our previous fMRI experiments demonstrated rough topological organization and potential subdivisions within the parietal face area using voxel volumes similar to those used in most cognitive fMRI experiments (Sereno and Huang, 2006). At a higher imaging resolution in the current study, we were able to confirm the existence of one or more topological

can/will be iteratively revised. For example, the left sROI of Subject 9 in Fig. S9 can be classified as Type 2.3v (a full complex model) or Type 2.0v (neglecting minor variations in the posterior parts). As another example, the left sROI of Subject 10 in Fig. S7 can be classified as Type 1.0 or Type 2.1, by slightly rotating the polar-angle gradient orientation (arrow) to match that in either type (Fig. 4B).

Within and across subjects, the most distinct and consistent feature of the parietal face area (VIP+ complex) is an anteriorly-centrally located upper face (or visual field) representation, which is adjoined by lower face (or visual field) representations ventrally (laterally) and/or dorsally (medially). This topology forms two potential subdivisions, VIPv (ventral) and VIPd (dorsal), in the VIP+ complex. These names were chosen to indicate that they are not necessarily homologous to subdivisions VIPm (medial) and VIPl (lateral) that have been proposed for macaque area VIP (Lewis and Van Essen, 2000a, 2000b). The lower visual field representation of VIPv extends ventrally/laterally into the anterior IPS to adjoin the parietal hand area (human area AIP), while the lower visual field representation of VIPd extends dorsally/medially to overlap with the parietal body areas at the superior end of the postcentral sulcus (Fig. 4; Huang et al., 2012). The lower visual field representations extending from either side of the VIP+ complex, particularly on the dorsal-medial side (VIPd), are present in almost every single-subject map (Fig. S9 and S10). These visual field representations provide additional topological contexts for locating the parietal face area amongst the neighboring unisensory and multisensory areas discussed above (Fig. 4A; also see group-average retinotopic maps in Huang and Sereno, 2018; Sereno and Huang, 2014).

Future studies

While the current study only mapped the polar angle coordinate of the contralateral hemiface and visual hemifield, our previous study of wide-field, average retinotopy including both polar angle and eccentricity has suggested that the parietal face area and nearby areas contain a representation that emphasizes the far periphery (Huang and Sereno, 2013). Future high-resolution mapping studies of eccentricity representation in the parietal face area using wide-field phase-encoded visual stimuli will be needed to refine these observations. Finally, two-dimensional somatotopic mapping of the face using high-density tactile stimuli delivered via a wearable grid will be required to determine how visual eccentricity relates to face somatotopic ‘eccentricity’ in the parietal face area in future studies (Chen et al., 2017; Huang and Sereno, 2010; Huang et al., 2012; Moulton et al., 2009; Sereno and Huang, 2010).

Conclusions

High-resolution imaging has identified the human parietal face area as a small region lying inside the superior postcentral sulcus and extending posteriorly to the upper bank of the anterior IPS, rather than in the depths of the IPS (as might be suggested by the name of macaque area VIP). This region is situated slightly lateral to the human LIP+ complex rather than medial to it (again, as might have been suggested by macaque area names LIP and VIP). Using voxel volumes smaller than typically used in cognitive neuroimaging studies, and small, closely-placed and hand-tuned surface coils, we were able to receive strong

BOLD signal changes from the parietal face area in response to both air puffs (physical contacts) delivered to the face and wide-field looming objects approaching the face (simulated contacts). The parietal face area's strong sensitivity to these multisensory stimuli in near-face space suggests that it plays an important role in detecting objects intruding into one's peripersonal space; and when they are perceived as potential threats, it is known to participate in promptly initiating and guiding defensive movements (Graziano and Cooke, 2006). Furthermore, the parietal face area plays an important role in multisensory integration and coordination of movements in near-face space (Avillac et al., 2007; Filimon et al., 2007, 2009; Sereno and Huang, 2014). Tactile and visual stimuli with a progressive change in polar angle around the face activated one or more maps of the contralateral hemiface and visual hemifield in the parietal face area. Across a large number of subjects in our current and previous studies, the topological organization of VIP+ complex consistently shows a anteriorly-centrally located upper face (or visual field) representation adjoined by lower face (or visual field) representations ventrally (laterally) and/or dorsally (medially), forming two potential subdivisions (VIPv and VIPd). Future studies are required to investigate their functional roles in perception and action in peripersonal space (Sereno and Huang, 2014).

Supplementary Material

Refer to Web version on PubMed Central for supplementary material.

Acknowledgments

This work was supported by the National Institutes of Health (R01 MH081990 to M.I.S. and R.-S.H.), Royal Society Wolfson Research Merit Award and Wellcome Trust to M.I.S., and UC San Diego Frontiers of Innovation Scholars Program (FISP) Project Fellowships to C.-f.C. We thank Eric C. Wong, Larry May, and other faculty and staff at the UCSD Center for Functional MRI for coil development and MRI support.

References

- Avillac M, Ben Hamed S, Duhamel JR, 2007 Multisensory integration in the ventral intraparietal area of the macaque monkey. *J. Neurosci.* 27, 1922–1932. [PubMed: 17314288]
- Avillac M, Deneve S, Olivier E, Pouget A, Duhamel JR, 2005 Reference frames for representing visual and tactile locations in parietal cortex. *Nat. Neurosci.* 8, 941–949. [PubMed: 15951810]
- Borra E, Belmalih A, Calzavara R, Gerbella M, Murata A, Rozzi S, Luppino G, 2008 Cortical connections of the macaque anterior intraparietal (AIP) area. *Cereb. Cortex* 18, 1094–1111. [PubMed: 17720686]
- Bremmer F, Klam F, Duhamel JR, Ben Hamed S, Graf W, 2002 Visual-vestibular interactive responses in the macaque ventral intraparietal area (VIP). *Eur. J. Neurosci.* 16, 1569–1586. [PubMed: 12405971]
- Bremmer F, Schlack A, Shah NJ, Zafiris O, Kubischik M, Hoffmann K, Zilles K, Fink GR., 2001 Polymodal motion processing in posterior parietal and premotor cortex: a human fMRI study strongly implies equivalencies between humans and monkeys. *Neuron* 29, 287–296. [PubMed: 11182099]
- Buxton RB, 2009 *Introduction to Functional Magnetic Resonance Imaging: Principles and Techniques*, second ed. Cambridge University Press, Cambridge United Kingdom ISBN: 978-0-521-89995-6.
- Cardin V, Smith AT, 2010 Sensitivity of human visual and vestibular cortical regions to egomotion-compatible visual stimulation. *Cereb. Cortex* 20, 1964–1973. [PubMed: 20034998]
- Chen A, DeAngelis GC., Angelaki DE, 2011 A comparison of vestibular spatiotemporal tuning in macaque parietoinsular vestibular cortex, ventral intraparietal area, and medial superior temporal area. *J. Neurosci.* 31, 3082–3094. [PubMed: 21414929]

- Chen CF, Kreutz-Delgado K, Sereno MI, Huang RS, 2017 Validation of periodic fMRI signals in response to wearable tactile stimulation. *NeuroImage* 150, 99–111. [PubMed: 28193488]
- Colby CL, Duhamel JR, Goldberg ME, 1993 Ventral intraparietal area of the macaque: anatomic location and visual response properties. *J. Neurophysiol.* 69, 902–914. [PubMed: 8385201]
- Cox RW, 1996 AFNI: software for analysis and visualization of functional magnetic resonance neuroimages. *Comput. Biomed. Res.* 29, 162–173. [PubMed: 8812068]
- Culham JC, Danckert SL, DeSouza JF, Gati JS, Menon RS, Goodale MA, 2003 Visually guided grasping produces fMRI activation in dorsal but not ventral stream brain areas. *Exp. Brain Res.* 153, 180–189. [PubMed: 12961051]
- Dale AM, Fischl B, Sereno MI, 1999 Cortical surface-based analysis. I. Segmentation and surface reconstruction. *NeuroImage* 9, 179–194. [PubMed: 9931268]
- Duhamel JR, Colby CL, Goldberg ME, 1991 Congruent representation of visual and somatosensory space in single neurons of monkey ventral intraparietal cortex (area VIP). in: Paillard J (Ed.), *Brain and Space*. Oxford University Press, Oxford, UK, pp. 223–236. ISBN: 978-0-19-854284-1.
- Duhamel JR, Colby CL, Goldberg ME, 1998 Ventral intraparietal area of the macaque: congruent visual and somatic response properties. *J. Neurophysiol.* 79, 126–136. [PubMed: 9425183]
- Eger E, Pinel P, Dehaene S, Kleinschmidt A, 2015 Spatially invariant coding of numerical information in functionally defined subregions of human parietal cortex. *Cereb. Cortex* 25, 1319–1329. [PubMed: 24293562]
- Engel SA, 2012 The development and use of phase-encoded functional MRI designs. *NeuroImage* 62, 1195–1200. [PubMed: 21985909]
- Fasold O, Heinau J, Trenner MU, Villringer A, Wenzel R, 2008 Proprioceptive head posture-related processing in human polysensory cortical areas. *NeuroImage* 40, 1232–1242. [PubMed: 18296073]
- Ferri S, Rizzolatti G, Orban GA., 2015 The organization of the posterior parietal cortex devoted to upper limb actions: An fMRI study. *Hum. Brain Mapp.* 36, 3845–3866. [PubMed: 26129732]
- Filimon F, Nelson JD, Hagler DJ, Sereno MI, 2007 Human cortical representations for reaching: mirror neurons for execution, observation, and imagery. *NeuroImage* 37, 1315–1328. [PubMed: 17689268]
- Filimon F, Nelson JD, Huang RS, Sereno MI, 2009 Multiple parietal reach regions in humans: cortical representations for visual and proprioceptive feedback during on-line reaching. *J. Neurosci.* 29, 2961–2971. [PubMed: 19261891]
- Fischl B, Sereno MI, Dale AM, 1999 Cortical surface-based analysis. II: Inflation, flattening, and a surface-based coordinate system. *NeuroImage* 9, 195–207. [PubMed: 9931269]
- Fischl B, Sereno MI, Tootell RB, Dale AM, 1999 High-resolution intersubject averaging and a coordinate system for the cortical surface. *Hum. Brain Mapp.* 8, 272–284. [PubMed: 10619420]
- Fisher NI, 1993 *Statistical Analysis of Circular Data*, first ed. Cambridge University Press, Cambridge, UK. ISBN: 978-051-15-6434-5. doi: [0.1017/CBO9780511564345](https://doi.org/10.1017/CBO9780511564345).
- Flechsig P, 1920 *Anatomie des menschlichen Gehirns und Rückenmarks auf myelogenetischer Grundlage*. Georg Thieme Verlag, Leipzig, Germany.
- Furlan M, Wann JP, Smith AT, 2014 A representation of changing heading direction in human cortical areas pVIP and CSv. *Cereb. Cortex* 24, 2848–2858. [PubMed: 23709643]
- Gattass R, Nascimento-Silva S, Soares JG, Lima B, Jansen AK, Diogo AC, Farias MF, Botelho MM, Mariani OS, Azzi J, Fiorani M, 2005 Cortical visual areas in monkeys: location, topography, connections, columns, plasticity and cortical dynamics. *Philos. Trans. R. Soc. Lond. B Biol. Sci.* 360, 709–731. [PubMed: 15937009]
- Graziano MS, Cooke DF, 2006 Parieto-frontal interactions, personal space, and defensive behavior. *Neuropsychologia* 44, 845–859. [PubMed: 16277998]
- Guipponi O, Wardak C, Ibarrola D, Comte JC, Sappey-Marinièr D, Pinede S, Ben Hamed S, 2013 Multimodal convergence within the intraparietal sulcus of the macaque monkey. *J. Neurosci.* 33, 4128–4139. [PubMed: 23447621]
- Hagler DJ, Jr., Riecke L, Sereno MI, 2007 Parietal and superior frontal visuospatial maps activated by pointing and saccades. *NeuroImage* 35, 1562–1577. [PubMed: 17376706]

- Helfrich RF, Becker HG, Haarmeier T, 2013 Processing of coherent visual motion in topographically organized visual areas in human cerebral cortex. *Brain Topogr.* 26, 247–263. [PubMed: 22526896]
- Hoffmann MB, Stadler J, Kanowski M, Speck O, 2009 Retinotopic mapping of the human visual cortex at a magnetic field strength of 7T *Clin. Neurophysiol.* 120, 108–116.
- Holt DJ, Cassidy BS, Yue X, Rauch SL, Boeke EA, Nasr S, Tootell RB, Coombs G, 3rd, 2014 Neural correlates of personal space intrusion. *J. Neurosci.* 34, 4123–4134. [PubMed: 24647934]
- Huang RS, Chen CF, Sereno MI, 2015 Neural substrates underlying the passive observation and active control of translational egomotion. *J. Neurosci.* 35, 4258–4267. [PubMed: 25762672]
- Huang RS, Chen CF, Tran AT, Holstein KL, Sereno MI, 2012 Mapping multisensory parietal face and body areas in humans. *Proc. Natl. Acad. Sci. U. S. A.* 109, 18114–18119. [PubMed: 23071340]
- Huang RS, Sereno MI, 2007 Dodecapus: An MR-compatible system for somatosensory stimulation. *NeuroImage* 34, 1060–1073. [PubMed: 17182259]
- Huang RS, Sereno MI, 2010 Two-dimensional somatotopic mapping of the human face Abstract in: 16th Annual Meeting of the Organization for Human Brain Mapping, Barcelona, Spain.
- Huang RS, Sereno MI, 2013 Bottom-up retinotopic organization supports top-down mental imagery. *Open Neuroimag. J.* 7, 58–67. [PubMed: 24478813]
- Huang RS, Sereno MI, 2018 Multisensory and sensorimotor maps. *Handb. Clin. Neurol* 151, 141–161. [PubMed: 29519456] [PubMed: 29519456]
- Jammalamadaka SR, SenGupta A, 2001 *Topics in Circular Statistics.* World Scientific Publishing Co, River Edge, New Jersey, USA. ISBN: 978–981-02–3778-3.
- Jastorff J, Begliomini C, Fabbri-Destro M, Rizzolatti G, Orban GA., 2010 Coding observed motor acts: different organizational principles in the parietal and premotor cortex of humans. *J. Neurophysiol.* 104, 128–140. [PubMed: 20445039]
- Konen CS, Kastner S, 2008 Representation of eye movements and stimulus motion in topographically organized areas of human posterior parietal cortex. *J. Neurosci.* 28, 8361–8375. [PubMed: 18701699]
- Lewis JW, Van Essen DC, 2000 Mapping of architectonic subdivisions in the macaque monkey, with emphasis on parieto-occipital cortex. *J. Comp. Neurol.* 428, 79–111. [PubMed: 11058226]
- Lewis JW, Van Essen DC, 2000 Corticocortical connections of visual, sensorimotor, and multimodal processing areas in the parietal lobe of the macaque monkey. *J. Comp. Neurol.* 428, 112–137. [PubMed: 11058227]
- Meier JD, Aflalo TN, Kastner S, Graziano MS, 2008 Complex organization of human primary motor cortex: a high-resolution fMRI study. *J. Neurophysiol.* 100, 1800–1812. [PubMed: 18684903]
- Moulton EA, Pendse G, Morris S, Aiello-Lammens M, Becerra L, Borsook D, 2009 Segmentally arranged somatotopy within the face representation of human primary somatosensory cortex. *Hum. Brain Mapp.* 30, 757–765. [PubMed: 18266215]
- Orban GA., Claeys K, Nelissen K, Smans R, Sunaert S, Todd JT, Wardak C, Durand JB, Vanduffel W, 2006 Mapping the parietal cortex of human and non-human primates. *Neuropsychologia* 44, 2647–2667. [PubMed: 16343560]
- Patel GH., Shulman GL, Baker JT, Akbudak E, Snyder AZ, Snyder LH, Corbetta M, 2010 Topographic organization of macaque area LIP. *Proc. Natl. Acad. Sci. U. S. A.* 107, 4728–4733. [PubMed: 20173093]
- Pitzalis S, Sdoia S, Bultrini A, Committeri G, Di Russo F, Fattori P, Galletti C, Galati G, 2013 Selectivity to translational egomotion in human brain motion areas. *PLoS One* 8, e60241. [PubMed: 23577096]
- Scheperjans F, Eickhoff SB, Homke L, Mohlberg H, Hermann K, Amunts K, Zilles K, 2008 Probabilistic maps, morphometry, and variability of cytoarchitectonic areas in the human superior parietal cortex. *Cereb. Cortex* 18, 2141–2157. [PubMed: 18245042]
- Scheperjans F, Hermann K, Eickhoff SB, Amunts K, Schleicher A, Zilles K, 2008 Observer-independent cytoarchitectonic mapping of the human superior parietal cortex. *Cereb. Cortex* 18, 846–867. [PubMed: 17644831]
- Schlack A, Sterbing-D’Angelo SJ, Hartung K, Hoffmann KP, Bremmer F, 2005 Multisensory space representations in the macaque ventral intraparietal area. *J. Neurosci.* 25, 4616–4625. [PubMed: 15872109]

- Schluppeck D, Glimcher P, Heeger DJ, 2005 Topographic organization for delayed saccades in human posterior parietal cortex. *J. Neurophysiol.* 94, 1372–1384. [PubMed: 15817644]
- Seelke AM, Padberg JJ, Disbrow E, Purnell SM, Recanzone G, Krubitzer L, 2012 Topographic maps within Brodmann's Area 5 of macaque monkeys. *Cereb. Cortex* 22, 1834–1850. [PubMed: 21955920]
- Sereno MI, Dale AM, Reppas JB, Kwong KK, Belliveau JW, Brady TJ, Rosen BR, Tootell RB, 1995 Borders of multiple visual areas in humans revealed by functional magnetic resonance imaging. *Science* 268, 889–893. [PubMed: 7754376]
- Sereno MI, Huang RS, 2006 A human parietal face area contains aligned head-centered visual and tactile maps. *Nat. Neurosci.* 9, 1337–1343. [PubMed: 16998482]
- Sereno MI, Huang RS, 2010 Finding somatosensory area boundaries in humans with the field sign technique Abstract in: 40th Annual Meeting of the Society for Neuroscience, San Diego, USA.
- Sereno MI, Huang RS, 2014 Multisensory maps in parietal cortex. *Curr. Opin. Neurobiol.* 24, 39–46. [PubMed: 24492077]
- Sereno MI, Lutti A, Weiskopf N, Dick F, 2012 Mapping the human cortical surface by combining quantitative T1 with retinotopy. *Cereb. Cortex* 23, 2261–2268. [PubMed: 22826609]
- Sereno MI, McDonald CT, Allman JM, 2015 Retinotopic organization of extrastriate cortex in the owl monkey -- dorsal and lateral areas. *Vis. Neurosci.* 32:e021. [PubMed: 26423343]
- Sereno MI, Pitzalis S, Martinez A, 2001 Mapping of contralateral space in retinotopic coordinates by a parietal cortical area in humans. *Science* 294, 1350–1354. [PubMed: 11701930]
- Smith AT, Wall MB, Thilo KV 2012 Vestibular inputs to human motion-sensitive visual cortex. *Cereb. Cortex* 22, 1068–1077. [PubMed: 21743097]
- Sunaert S, Van Hecke P, Marchal G, Orban GA., 1999 Motion-responsive regions of the human brain. *Exp. Brain Res.* 127, 355–370. [PubMed: 10480271]
- Swisher JD, Halko MA, Merabet LB, McMains SA, Somers DC, 2007 Visual topography of human intraparietal sulcus. *J. Neurosci.* 27, 5326–5337. [PubMed: 17507555]
- Wall MB, Smith AT, 2008 The representation of egomotion in the human brain. *Curr. Biol.* 18, 191–194. [PubMed: 18221876]

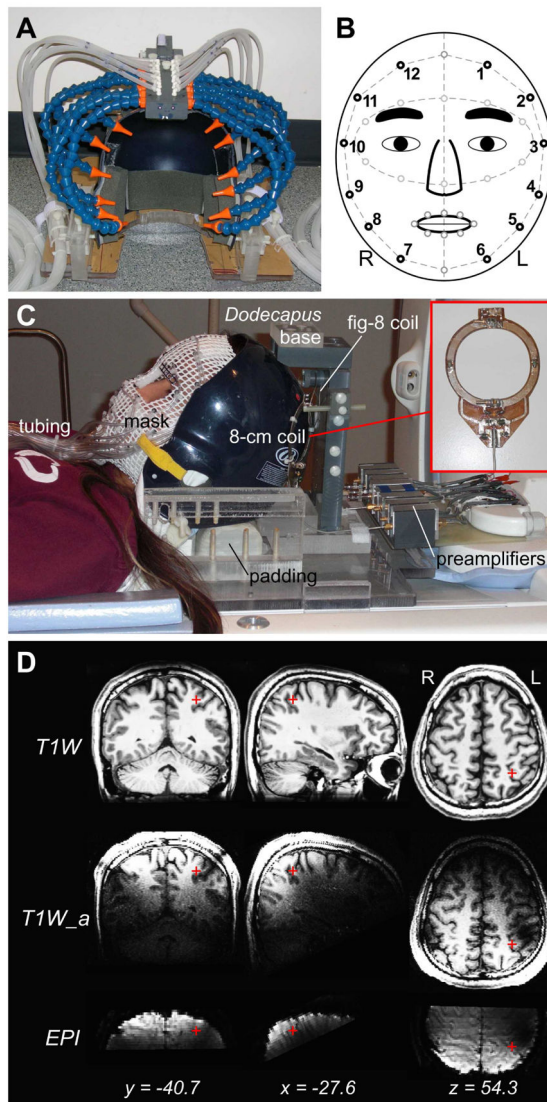


Figure 1. MRI-compatible devices for radio-frequency signal acquisition and tactile stimulation. **(A)** Dodecapus manifold mounted above a baseball helmet for Experiment 1. **(B)** A schematic of stimulation sites (black circles) on the face in both experiments. **(C)** Integration of wearable tactile stimulation (mask) and surface coils for Experiment 2. **(D)** Location of the parietal face area (red cross) in the left hemisphere of Subject 1. T1W: T1-weighted structural images (average of two image sets); T1W_a: T1-weighted alignment images; EPI: functional images.

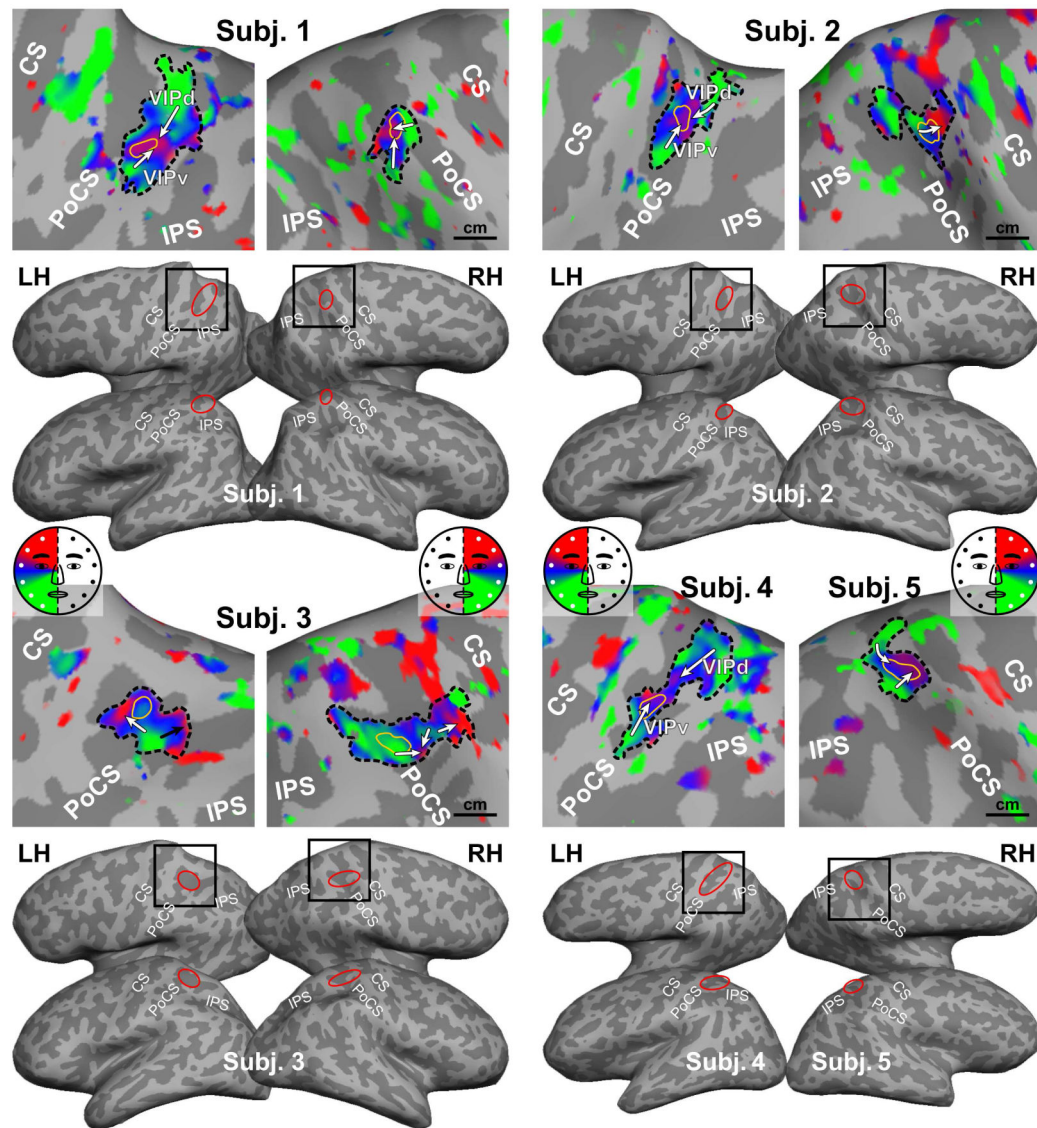


Figure 2. Somatotopic maps of five subjects in Experiment 1. All maps were rendered with the same statistical threshold ($F_{2230} = 3.035$, $p = 0.05$, uncorrected). Black box: location of each close-up map on the dorsal-lateral cortical surface; Red ellipse: location of the parietal face area on each cortical surface; Dashed black contour: an sROI of the parietal face area; Thin yellow contour: the peak activation region within an sROI; A white or black arrow: a lower-to-upper progression of the contralateral hemiface representation (see color wheel); CS: central sulcus; PoCS: postcentral sulcus; IPS: intraparietal sulcus; LH/RH: left/right hemisphere.

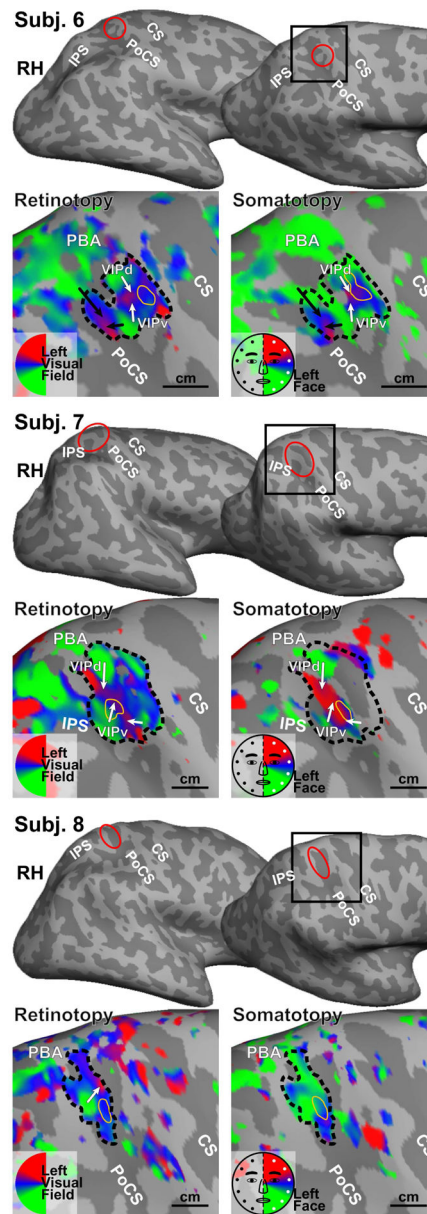


Figure 3. Retinotopic and somatotopic maps of three subjects in Experiment 2. All maps were rendered with the same statistical threshold ($F_{2, 230} = 3.035$, $p = 0.05$, uncorrected). Each sROI is outlined in the retinotopic map and then superimposed on the somatotopic map. PBA: parietal body areas. Other conventions as in Fig. 2.

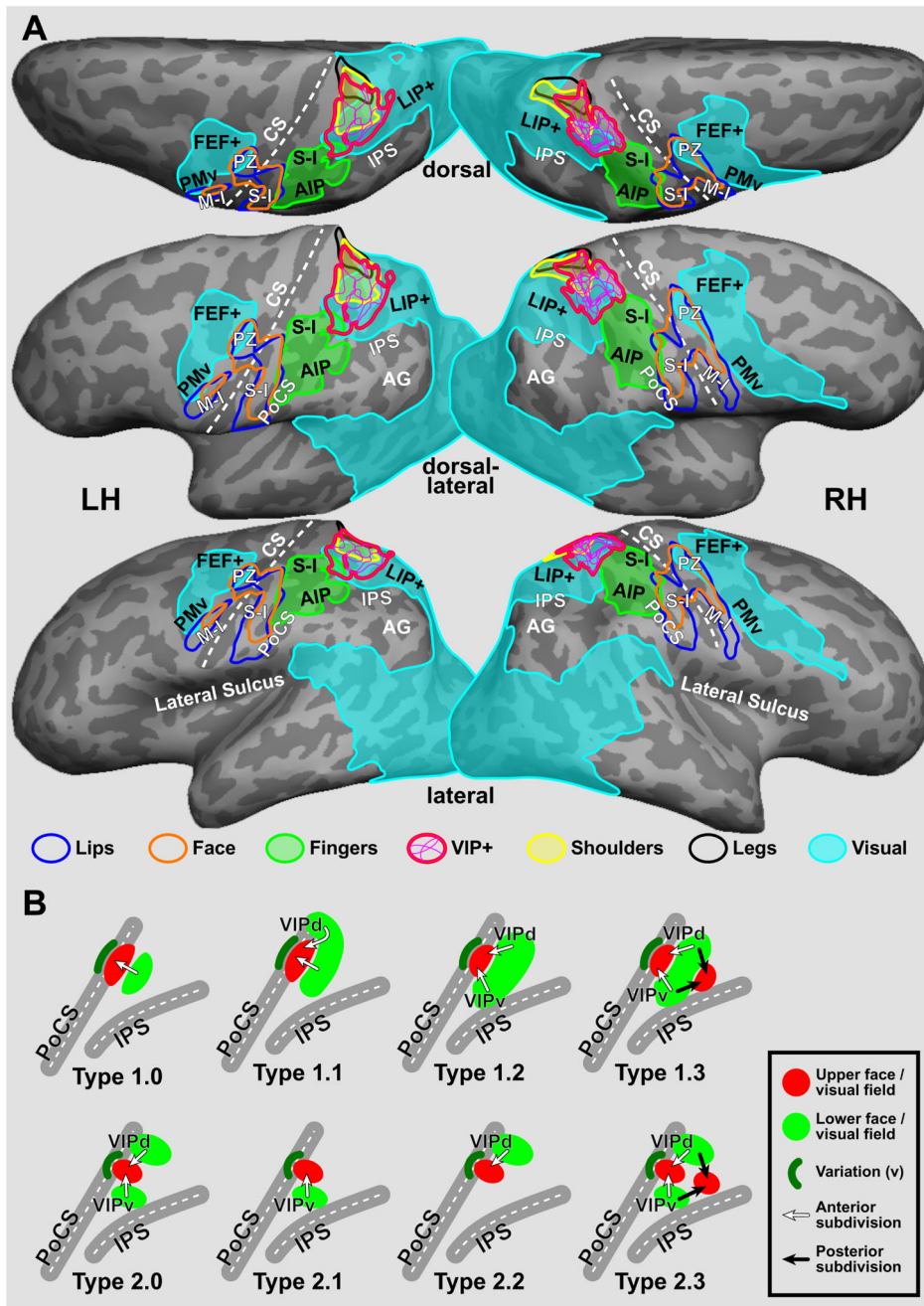


Figure 4. Location, extent, and models of the parietal face area. (A) The cortical surfaces of Subject 1 were overlaid with contours of the parietal face area sROI spherically morphed from four left hemispheres and seven right hemispheres of eight subjects in Figs. 2 and 3. A thin magenta contour indicates the border of a single-subject sROI, and a thick magenta contour indicates the common external border of all sROI. Group-average contours of lip, face, and finger (hand) representations in the primary somatosensory cortex (S-I) and parietal body areas (PBA; including shoulder and leg representations) were obtained by passive tactile stimulation in previous studies (Huang et al., 2012; Huang and Sereno, 2007). Group-

average contours of video-driven visual cortex were obtained from Huang and Sereno (2018). **(B)** Schematic topological models of the parietal face area (VIP+ complex) in the left hemisphere (see single-subject maps in Fig. S7-S10 and map classification in Table 3). FEF+: frontal eye field complex; PZ: polysensory zone; PMv: ventral premotor cortex; M-I: primary motor cortex; AIP: anterior intraparietal area; LIP+: human homologue of macaque area LIP; AG: angular gyrus. Other abbreviations as in text and Fig. 2.

Author Manuscript

Author Manuscript

Author Manuscript

Author Manuscript

Table 1.

Measurements and statistics of sROIs in Experiment 1.

Subject / hemisphere	sROI		Peak activation region					Average <i>p</i> -value*
	Surface area (mm ²)	Vertices	Total volume (mm ³)	Surface area (mm ²)	Voxels	Average Talairach coordinates		
1 / LH	361	606	1276.4	14.8	8	(-27.6, -40.7, 54.3)	6.6×10 ⁻¹⁰	
1 / RH	121.1	300	609.6	14.7	13	(33.7, -35.8, 53.5)	6.4×10 ⁻¹¹	
2 / LH	173.9	313	666.8	14	10	(-28.6, -39.7, 61.0)	2.0×10 ⁻¹⁰	
2 / RH	114.2	262	508	19	14	(27.0, -41.9, 56.3)	2.9×10 ⁻¹¹	
3 / LH	192.2	220	393.7	16.2	7	(-21.5, -38.1, 58.3)	4.6×10 ⁻⁷	
3 / RH	287.7	641	1270	22.6	7	(26.3, -37.8, 50.4)	1.9×10 ⁻¹⁶	
4 / LH	275.5	532	1085.9	18.1	9	(-19.7, -35.8, 39.7)	9.3×10 ⁻⁵	
5 / RH	144.5	286	831.9	33.6	7	(23.1, -39.5, 70.5)	1.1×10 ⁻⁹	

See corresponding sROI (dashed black contours) and peak activation regions (thin yellow contours) in Fig. 2. Volume per voxel: 6.35 mm³;

* : FDR corrected.

Table 2.

Measurements and statistics of sROIs in Experiment 2.

Subject/ modality	sROI		Peak activation region			Visual-tactile alignment				
	Surface area (mm ²)	Vertices	Voxels	Surface area (mm ²)	Total volume (mm ³)	Voxels	Average Talairach coordinates	Average <i>p</i> -value [*]	Overlapping vertices (%) [†]	Circular correlation coefficient, <i>p</i> -value [‡]
6 / Visual	222.3	545	172	15.6	928.8	18	(34.3, -37.5, 64.6)	9.7×10^{-10}	82.2	$0.38, p < 4.03 \times 10^{-11}$
6 / Tactile				14		16	(31.1, -38.0, 65.8)	1.3×10^{-14}		
7 / Visual	496.4	1012	118	13.5	637.2	8	(32.1, -41.8, 62.5)	7.5×10^{-15}	30.93	$0.66, p = 0$
7 / Tactile				20.3		10	(35.0, -43.3, 63.1)	3.8×10^{-5}		
8 / Visual	176.6	347	96	14.9	518.4	13	(24.0, -36.9, 57.7)	1.0×10^{-5}	78.1	$0.06, p = 1$ (n.s.)
8 / Tactile				14.1		10	(24.3, -37.3, 58.1)	0		

See corresponding sROI (dashed black contours) and peak activation regions (thin yellow contours) in Fig. 3. Volume per voxel: 5.4 mm³;

* : FDR corrected;

† : percentage of vertices in an sROI with $p < 0.05$ (uncorrected) in both modalities;

‡ : Bonferroni-corrected *p*-value estimated from overlapping vertices only; n.s. not significant.

Table 3.

Classification of single-subject maps by topological types.

Type	Modality	Figure	Subject #
1.0	Tactile	S7	9, 10, 11
		S8	2 ^v , 2 ^v , 9, 12 ^v , 13 ^v , 14 ^v
	Visual	S10	5 ^v , 8 ^v , 12
1.1	Tactile	S7	12
		S8	5, 5
	Visual	S9	13 ^v
	Visual	S10	1 ^v , 2 ^v , 14 ^v , 17 ^v , 19 ^v
1.2	Visual	S9	11, 12 ^v , 25 ^v
		S10	9, 11, 18, 25 ^v
1.3	Visual	S9	5 ^v , 19 ^v , 20
2.0	Tactile	S7	1, 1, 2 ^v , 4
		S8	7 ^v , 11 ^v
	Visual	S9	1, 2 ^v , 4, 15
		S10	7 ^v , 13 ^v , 16 ^v , 20 ^v
2.1	Tactile	S8	1 ^v , 1 ^v
2.2	Tactile	S7	2 ^v
	Visual	S9	22, 24 ^v
2.3	Tactile	S7	3 ^v , 3 ^v
		S8	6 ^v
	Visual	S9	3 ^v , 9 ^v , 10, 16 ^v , 17, 18, 21 ^v , 23 ^v
		S10	6 ^v , 24 ^v , 26 ^v
None	Tactile	S7	13, 14
		S8	3, 3, 8, 10
	Visual	S9	14
		S10	3, 10, 15, 21, 23

See topological types in Fig. 4B. Subject #: head-coil session; Subject #: surface-coil session; Subject #^v or #^v: type variation.